

Lab on a Chip

Accepted Manuscript



This is an *Accepted Manuscript*, which has been through the Royal Society of Chemistry peer review process and has been accepted for publication.

Accepted Manuscripts are published online shortly after acceptance, before technical editing, formatting and proof reading. Using this free service, authors can make their results available to the community, in citable form, before we publish the edited article. We will replace this *Accepted Manuscript* with the edited and formatted *Advance Article* as soon as it is available.

You can find more information about *Accepted Manuscripts* in the [Information for Authors](#).

Please note that technical editing may introduce minor changes to the text and/or graphics, which may alter content. The journal's standard [Terms & Conditions](#) and the [Ethical guidelines](#) still apply. In no event shall the Royal Society of Chemistry be held responsible for any errors or omissions in this *Accepted Manuscript* or any consequences arising from the use of any information it contains.

Multiplexed Actuation Using Ultra Dielectrophoresis for Proteomics Applications: A Comprehensive Electrical and Electrothermal Design Methodology

Sam Emaminejad^{,1,2,3}, Robert W. Dutton¹, Ronald W. Davis^{2,3} and Mehdi Javanmard^{*,2,3}*

¹ Dept. of Electrical Engineering, Stanford University, Stanford, CA

² School of Medicine, Stanford University, Stanford, CA, USA.

³ Stanford Genome Technology Center, Palo Alto, CA

* To whom correspondence should be addressed. E-mail: same@stanford.edu (S.E.),
mehdij@stanford.edu (M.J.)

Abstract

In this work, we present a methodological approach to analyze an enhanced dielectrophoresis (DEP) system from both a circuit analysis and an electrothermal view points. In our developed model, we have taken into account various phenomena and constraints such as voltage degradation (due to the presence of the protecting oxide layer), oxide breakdown, instrumentation limitations, and thermal effects. The results from this analysis are applicable generally to a wide variety of geometries and high voltage microsystems. Here, these design guidelines were applied to develop a robust electronic actuation system to perform a multiplexed bead-based protein assay. To carry out the multiplexed functionality, along a single microfluidic channel, an array of proteins is patterned, where each element is targeting a specific secondary protein coated on micron-sized beads in the subsequently introduced sample solution. Below each element of the array, we have a pair of addressable interdigitated electrodes. By selectively applying voltage at the terminals of each interdigitated electrode pair, the enhanced DEP, or equivalently ‘ultra’-DEP (uDEP) force detaches protein-bound beads from each element of the array, one by one, without disturbing the bound beads in the neighboring regions. The detached beads can be quantified optically or electrically downstream. For proof of concept, we illustrated 16-plex actuation capability of our device to elute micron-sized beads that are bound to the surface through anti-IgG and IgG interaction which is on the same order of magnitude in strength as typical antibody-antigen interactions. In addition to its application in multiplexed protein analysis, our platform can be potentially utilized to statistically characterize the strength profile of biological bonds, since the multiplexed format allows for high throughput force spectroscopy using the array of uDEP devices, under the same buffer and assay preparation conditions.

Keywords:

Atomic Layer Deposition, Thin film oxide, Negative Dielectrophoresis, Electrokinetic Actuation, Protein assay

Introduction

Despite the immense progress that has been made in discovery and validation of genomics over the last decade, proteomic biomarkers have lagged behind considerably compared to their genomic counterparts because of the inherent limitations in sensitivity of protein assays and also the ability to perform multiplexed detection of proteins and study of protein-protein interactions. Fluorescence based techniques such as ELISA¹ and also protein microarrays² have served as the gold standard for protein detection. Electronic detection systems are also showing promise for label free detection³⁻⁶. More recently, bead based protein assays have begun emerging as alternatives to fluorescent assays due to several advantages that beads have over fluorophores. The use of beads has been shown to enhance sensitivity in protein assays given the fact that the bead itself serves to amplify the detection signal, whether electrical,⁷⁻¹⁰ optical,¹¹ or magnetic.¹²⁻¹⁴ Another advantage, given the micron size of beads is that one can better control the force applied to beads and thus measure the affinity of biomolecules' interactions. This has previously been shown using shear force¹⁵, optical tweezers¹⁶, magnetic tweezers¹⁷, and more recently electrokinetic forces¹⁸⁻²¹. Electronic force provides the advantage of scalability and precise addressability when multiplexing. With precise voltage control, one also has better control over the applied force compared to the alternative techniques mentioned. The difficulty with electrokinetic forces lies in the inherent weakness of these forces (1-10 pN) compared to typical biomolecular interactions (~nN). This two order of magnitude gap resulted from a lack of proper modeling of the electrical and thermal behavior of high voltage dielectrophoretic systems. In this manuscript, we demonstrate the ability to study protein-protein interactions in multiplexed format, and more importantly we develop a complete model along with methodological design guidelines for high voltage dielectrophoretic systems coated with thin film insulative layers.

Previously, with the aid of negative dielectrophoresis (nDEP) force in conjunction with shear force and eluting agent, we demonstrated a switch-like functionality to elute specifically bound beads from the surface²¹. The role of the eluting agent, at an optimal concentration, was to sufficiently weaken the

bindings such that the nDEP force would be able to push the specifically bound beads off the surface. While the use of the eluting agent assisted with establishing the switching functionality of nDEP as a proof of concept, its use was not desirable in performing multiplexed assay along a single channel. To eliminate the need for the eluting agent, we focused on enhancing the nDEP force significantly, primarily through fabricating high voltage tolerant corrosion proof electrodes that enabled us to apply high ac voltages at the electrodes. This was achieved by depositing a protective pinhole free nanometer-scale thin film layer on electrodes, using Atomic Layer Deposition (ALD).

The ultra thin nature of the film as well as excitation of voltage at high frequency allowed us to capacitively couple the electrodes to the electrolyte. This minimized the undesired voltage drop across the oxide layer; a phenomenon from which previously proposed solutions suffered due to deposition of thick oxide layers. As a result, we ultimately enhanced the strength of DEP by two orders of magnitude. Development of this localized electrokinetic actuator has expanded the horizon of utilizing DEP in various microfluidic applications. Just recently, the application of ‘ultra’ DEP (uDEP) was demonstrated in a two-component on-chip particle filtering platform that is used for the depletion of cells and highly abundant serum proteins in blood.²² Here, we utilize an array of uDEP electrodes to implement a multiplexed bead-based protein assay, which can be used as a rapid and inexpensive method for screening a panel of proteins in a given sample.

However, prior to implementation of the envisioned platform, a careful circuit and electrothermal analysis is required in order to understand the relevant parameters and constraints in the design space, with the goal of maximizing the DEP force in our system. Therefore, we first present a methodological approach to analyze an enhanced dielectrophoresis (DEP) system accordingly. In our developed model, we have taken into account various phenomena and constraints such as voltage degradation (due to the presence of the protecting oxide layer), oxide breakdown, instrumentation limitations, and thermal effects. The results from this analysis are applicable to a wide variety of geometries and generally high

voltage microsystems. Here, they were applied to develop our envisioned electronic actuation system to perform a multiplexed bead-based protein assay.

To implement the multiplexed platform, as illustrated in Figure 1, along a single microfluidic channel, an array of proteins is patterned, where each element is targeting a specific secondary protein coated on micron-sized beads in the subsequently introduced sample solution. Below each element of the array, we have a pair of addressable interdigitated electrodes (IDE). By selectively applying voltage at the terminals of each IDE pair, the enhanced DEP force detaches protein-bound beads from each element of the array, one by one, without disturbing the bound beads in the neighboring regions. The detached beads can be quantified optically or electrically downstream. It is worth mentioning that using IDE as the electrode configuration of choice provided the periodicity and scalability needed to maximize the analyte capture and actuation zone for each element of our array. For proof of concept, we illustrated 16-plex actuation capability of our device to elute micron-sized beads that are bound to the surface through anti-IgG and IgG interaction which is on the same order of magnitude in strength as typical antibody-antigen interactions.

In addition to its application in multiplexed protein analysis, our platform can potentially enhance the capability of DEP in statistical characterization of the strength profile of biological bonds. The multiplexed format enables performing force spectroscopy of multiple interactions independently in a single channel; minimizing inter-experiment variations that originate from disparities in buffer conditions and assay preparation steps. This approach can be particularly useful when characterizing specific vs. non-specific interactions simultaneously as it facilitates, under the same buffer condition, independent actuation of beads that are specifically bound to the functionalized electrodes (with pre-immobilized antibodies), as well as non-specifically bound beads that are attached to the ‘control’ (non-functionalized) electrodes. This ultimately helps with establishing optimal buffer conditions.

Theoretical Background and Design Methodology

Circuit Model

As mentioned earlier, to prevent the electrode corrosion we deposited a protective pinhole free nanometer-scale thin ALD oxide on our IDEs. From a circuit modeling perspective this insulative thin layer acts as a capacitance in series with the double-layer capacitance at the interface of the electrode-oxide-electrolyte interface, where the oxide capacitance due to its larger thickness and lower effective dielectric constant dominates. As shown in Figure 2(a), the oxide capacitance C_{ox} at each electrode terminal forms a voltage divider with the conductive solution buffer of resistance R . Formation of this voltage divider effectively causes an unwanted voltage drop V_C across the oxide films at each terminal end, resulting in degradation of electric field and available DEP force inside the solution buffer:

$$V_C = \left| \frac{1}{1 + j2\pi f \frac{RC_{ox}}{2}} \right| \frac{V_{app}}{2} \quad (1)$$

As verified previously¹⁹ for a pair of neighboring electrodes, the oxide capacitance C_{ox} to the first order can be modeled as a parallel plate capacitance, with permittivity ϵ_{ox} , thickness t_{ox} , and area A_{el} (bound by the transverse width w_{ch} of the channel and width w_{el} of an electrode, equal to $w_{el} \times w_{ch}$). Similarly, the buffer solution can be approximated as resistance R with conductivity σ and length s_{el} equal to that of the conductivity of the buffer and spacing of the electrodes respectively. The effective cross section of R can be estimated as A_{el} ¹⁹. Therefore, V_C can be approximated as:

$$V_C \cong \left| \frac{1}{1 + j\pi f \left(\frac{s_{el}}{\sigma A_{el}} \right) \left(\frac{\epsilon_0 \epsilon_{ox} A_{el}}{t_{ox}} \right)} \right| \frac{V_{app}}{2} = \left| \frac{1}{1 + j\pi f \left(\frac{s_{el}}{\sigma} \right) \left(\frac{\epsilon_0 \epsilon_{ox}}{t_{ox}} \right)} \right| \frac{V_{app}}{2} \quad (2)$$

To extend the circuit model of the interface of a pair of neighboring electrodes and model the interdigitated configuration with n pair of electrodes, we simply need to consider the parallel combination of n neighboring electrode pairs. Regardless, the derived expression for V_C and our subsequent analysis (for the most part) remain unchanged, since the product RC_{ox} stays the same, in the parallel configuration. Equation 2 can further be re-organized and simplified to better capture the role of

the geometrical (electrode spacing and oxide thickness) and operational (excitation frequency and buffer conductivity) parameters in V_C :

$$V_C \cong \frac{1}{\sqrt{1 + \left[\pi \epsilon_0 \epsilon_{ox} s_{el} \left(\frac{f}{\sigma} \right) \left(\frac{1}{t_{ox}} \right) \right]^2}} \frac{V_{app}}{2} = \frac{1}{\sqrt{1 + \alpha^2}} \frac{V_{app}}{2} \quad (3)$$

where we set $\alpha = \left[\pi \epsilon_0 \epsilon_{ox} s_{el} \left(\frac{f}{\sigma} \right) \left(\frac{1}{t_{ox}} \right) \right]$ to simplify the ensuing derivations. Similarly, for the given voltage divider, we can derive the voltage V_R across the buffer that enables the DEP force:

$$V_R \cong \frac{1}{\sqrt{1 + \left[\left(\frac{1}{\pi \epsilon_0 \epsilon_{ox} s_{el}} \right) \left(\frac{\sigma}{f} \right) t_{ox} \right]^2}} V_{app} = \frac{1}{\sqrt{1 + \left(\frac{1}{\alpha} \right)^2}} V_{app} \quad (4)$$

If we are to minimize the undesired voltage drop V_C (or equivalently maximize V_R), and apply the most of V_{app} directly across the buffer, we need to maximize α . In this expression and for our case, ϵ_{ox} is 3.9, corresponding to the dielectric constant of SiO_2 that we used as the ALD oxide layer. We had the more favorable option of using higher dielectric constant ALD oxides Al_2O_3 ($\epsilon_{ox, \text{Al}_2\text{O}_3} \sim 5$), and HfO_2 ($\epsilon_{ox, \text{HfO}_2} \sim 20$), however, from implementation point of view, our efforts in providing a strong PDMS-substrate bond (amenable to microfluidic pressure driven application) was only successful for the case of SiO_2 . Furthermore, referring to the derived expression, it can be concluded that s_{el} can be increased to reduce the undesired voltage drop. However, one should keep in mind that this is achieved at the cost of weakening the electric field strength and subsequently the DEP force; hence its defeats our original purpose.

As a result, the effective design knobs for maximizing V_R are the operational parameters, f , σ , and V_{app} as well as the fabrication parameter t_{ox} . The value of f can be simply varied by exciting the electrodes at the desirable frequency, typically in the range of up to 10-100 MHz (for a high voltage excitation system). Moreover, σ can be set, if not restricted by prior implementation requirements, by using a solution buffer with the conductivity of interest (in the wash step), practically ranging from 0.1 mS/m (corresponding to that of the deionized (DI) water) to approximately 10 S/m (NaCl-concentrated-Phosphate Buffered Saline (PBS)²³). With regards to the practical range for t_{ox} , using techniques such as

plasma enhanced chemical vapor deposition we can deposit oxide films of thicknesses down to 50 nm. To deposit thinner oxides, we have to resort to ALD which can typically provide pinhole free oxide layers down to a few nanometers.

In our design space, we need to take into account various constraints. The first constraint is imposed by the electric field oxide breakdown of our ALD thin film ($E_{BR,ox}$), which sets an upper bound on the electric field which can be dropped across the thin film (*i.e.* $E_{ox} = \frac{V_C}{t_{ox}} < E_{BR,ox}$):

$$E_{ox} = \frac{1}{\sqrt{1+\alpha^2}} \frac{V_{app}}{2t_{ox}} < E_{BR,ox} \quad (5)$$

The oxide breakdown criterion effectively limits our ability to simply increase V_{app} in order to compensate for the degrading effect of the oxide film. We denote $V_{app,max}$ as the maximum voltage that can be applied at the electrodes, without exceeding the design constraints. To meet the oxide breakdown criterion (formulated by inequality 5) $V_{app,max}$ can be computed as:

$$V_{app,max} \cong 2E_{BR,ox}t_{ox}\sqrt{1+\alpha^2} \quad (6)$$

Combining equations 4 and 6, yields the expression for maximum voltage $V_{R,max}$ that can be applied across the buffer without causing oxide breakdown:

$$V_{R,max} \cong 2E_{BR,ox}t_{ox} \sqrt{\frac{1+\alpha^2}{1+\frac{1}{\alpha^2}}} = 2E_{BR,ox}\pi\epsilon_0\epsilon_{ox}S_{el} \left(\frac{f}{\sigma}\right) \quad (7)$$

Equation 7 from practical standpoint seems counter-intuitive and also contradictory to our motivation of maximizing the applied voltage across the buffer, as it shows our ability to apply $V_{R,max}$ is independent of the oxide thickness. Additionally, it implies that we can indefinitely improve $V_{R,max}$, by increasing $\left(\frac{f}{\sigma}\right)$. This conundrum can be resolved by taking into account the instrumentation limitation.

From instrumentation point of view, our ability to deliver high voltages at the electrodes is constrained by the maximum voltage amplitude at the output of the signal generator $V_{ac,max}$, as well as the maximum ac current $I_{ac,max}$ that the signal generator can deliver to establish the desired voltage across the electrodes. The former translates to $V_{R,max} = \frac{V_{ac,max}}{\sqrt{1+\left(\frac{1}{\alpha}\right)^2}}$, while the latter sets $V_{R,max} = I_{ac,max} \left(\frac{R}{n}\right) \cong$

$I_{ac,max} \left(\frac{s_{el}}{n\sigma A_{el}} \right)$ (recall n is the number of electrode pairs in our interdigitated configuration). Therefore, to accommodate for this limitations we revise $V_{app,max}$ and $V_{R,max}$ expressions accordingly:

$$V_{app,max} = \min \left\{ 2E_{BR,ox} t_{ox} \sqrt{1 + \alpha^2}, V_{ac,max}, I_{ac,max} \left(\frac{s_{el}}{n\sigma A_{el}} \right) \sqrt{1 + \left(\frac{1}{\alpha} \right)^2} \right\} \quad (8)$$

$$V_{R,max} = \min \left\{ 2E_{BR,ox} \pi \epsilon_0 \epsilon_{ox} s_{el} \left(\frac{f}{\sigma} \right), \frac{V_{ac,max}}{\sqrt{1 + \left[\left(\frac{1}{\pi \epsilon_0 \epsilon_{ox} s_{el}} \right) \left(\frac{\sigma}{f} \right) t_{ox} \right]^2}}, I_{ac,max} \left(\frac{s_{el}}{n\sigma A_{el}} \right) \right\} \quad (9)$$

To better visualize the design space, in Figures 2(b) and (c) we respectively illustrated $V_{R,max}$ for $t_{ox} = 10$ nm and 1000 nm that can be achieved, while meeting the oxide breakdown criterion ($E_{BR,ox} = E_{BR,ALD}$ $s_{iO_2} = 1$ V/nm) and instrumentation limitation (here assumed $V_{ac,max} = 100$ V, $I_{ac,max} = 0.2$ A), in the f vs. σ space. Here we assumed the same IDE geometry as that outlined in ‘Fabrication’ section. As can be seen from these figures, deposition of thin oxide layer (10 nm vs. 1000 nm) provides more flexibility (i.e. wider range of frequency and buffer conductivity conditions) for applying the most of V_{app} directly across the buffer.

In addition to the electrical modeling aspects that are discussed above, we need to study the thermal behavior of our high ac voltage microsystem. Previously, simplified thermal models for similar electrode-electrolyte configurations have been proposed.^{24, 25} In this work, we build on these efforts and propose a comprehensive model which complements the previous works with more rigorous formulation of temperature increase. This, in turn helps to quantify the thermal constraints in our system more accurately.

Assuming the homogeneous buffer solution in the channel undergoes no phase changes, the general heat equation can be written as:

$$q_g(\mathbf{r}, t) + \nabla \cdot k \nabla T = \rho C_p \frac{\partial T}{\partial t} \quad (10)$$

where q_g is the rate of internal heat density generation, T is the temperature, and ρ , C_p , and k are density, specific heat, and thermal conductivity of the solution buffer respectively. In our case, heat

density generation is due to Joule heating caused by the electric field inside the microchannel ($q_g = \sigma E_{RMS}^2$). Assuming steady state and negligible convective effects (low Rayleigh number), the heat equation can be reduced to:

$$k\nabla^2 T + \sigma E_{RMS}^2 = 0 \quad (11)$$

In our high ac voltage system, Joule heating may increase the temperature considerably in the channel, proportional to the generated power density σE_{RMS}^2 . Generally, the increase of temperature reduces the solubility of gas in liquid, and in particular, causes bubble formation in microfluidic devices and disrupts the intended operation. This directly limits our ability to apply high voltages in our design space, and more specifically sets an upper-bound on the term σV_R^2 .

To illustrate the proportionality of the raise in temperature with the generated power density, it helps to analyze a simplified and first-order thermal model of our device. As the channel transverse width is larger than the width and spacing of the electrodes (*i.e.* $w_{ch} > w_{el}, s_{el}$) and given the periodicity format of the IDE pair, we may assume a one-dimensional conduction in the direction normal to the plane of the electrodes. Furthermore, we assume that the electrodes are patterned on a substrate with thickness t_{sub} and thermal conductivity of k_{sub} , where the bottom of the substrate is kept at constant ambient temperature of T_∞ . The side-walls and the ceiling of the channel can be considered as perfect thermal insulators (implying $\frac{dT}{dx} = 0$ at the boundary), as in our context, the thermal conductivity of the PDMS housing is substantially smaller than that of the bottom glass substrate. For simplicity, we further suppose uniform internal heat generation of $q_g = \sigma E_{RMS}^2 \cong \sigma \left[\left(\frac{1}{2} \right) \left(\frac{V_R}{s_{el}} \right)^2 \right]$ in an effective volume confined by the channel's sidewalls and surface, and a plane that is at the distance w_{el} above the surface (corresponding to the volume with relatively strong electric field). Under the above assumptions, and using equation 11, temperature increase ΔT in the channel with respect to T_∞ can be estimated as:

$$\begin{aligned} \Delta T &\cong \left(\frac{w_{el}}{2k_m} + \frac{t_{sub}}{k_{sub}} \right) q_g w_{el} \\ &\cong \left(\frac{w_{el}}{2k_m} + \frac{t_{sub}}{k_{sub}} \right) \sigma \left[\left(\frac{1}{2} \right) \left(\frac{V_R}{s_{el}} \right)^2 \right] w_{el} \end{aligned}$$

$$\cong \frac{t_{sub} \gg w_{el}}{2} \left(\frac{t_{sub} w_{el}}{s_{el}^2} \right) \left(\frac{\sigma}{k_{sub}} \right) V_R^2 \quad (12)$$

$$\Delta T = \left(\frac{1}{\beta} \right) \left(\frac{\sigma}{k_{sub}} \right) V_R^2 \quad (13)$$

where $\beta = 2 \left(\frac{s_{el}^2}{t_{sub} w_{el}} \right)$ captures the role of geometrical dimensions. Here, we should note that for more accurate results, the exact coplanar IDE pair geometry (where electric-field, and thus, Joule heating are non-uniform) needs to be analyzed. In any case, our first order model correlates well with our COMSOL (COMSOL, Stockholm, Sweden) simulations of coplanar IDE pair (Figure 3(a)), demonstrating the proportionality of the temperature increase with Joule heating and imposing an upper-bound on σV_R^2 in our design space. To precisely model the thermal behavior of the coplanar configuration, β can be adjusted through calibration with simulation accordingly (in our case increased by $\sim 30\%$). The discrepancy between simulation and analytical model in determining the value of β is mainly due to the method of approximation used to model the non-uniform electric field. To compare the exact electric field solution computed by the COMSOL simulation with that obtained from our analytical model see the supplementary information.

Assuming bubble formation disrupts our operation upon temperature increase of ΔT_{max} (practically $\sim 40\text{-}50$ °C when operating at room temperature), we can rearrange equation 13, to obtain the expression for thermally limited maximum voltage $V_{R,max,th}$ that can be applied across the buffer without causing bubble formation:

$$V_{R,max,th} \cong \sqrt{\beta \left(\frac{k_{sub}}{\sigma} \right) \Delta T_{max}} \quad (14)$$

To sum up, based on the developed electrical and thermal models, in our high voltage corrosion-proof microsystem our ability to apply DEP-enabling voltage directly across the solution is constrained by oxide breakdown, instrumentation limitation, and temperature increase. Equation 15 below includes all these limiting phenomena, in a unified expression:

$$V_{R,max} = \min \left\{ 2E_{BR,ox} \pi \epsilon_0 \epsilon_{ox} S_{el} \left(\frac{f}{\sigma} \right), \frac{V_{ac,max}}{\sqrt{1 + \left(\frac{1}{\alpha} \right)^2}}, I_{ac,max} \left(\frac{S_{el}}{n\sigma A_{el}} \right), \sqrt{\beta \left(\frac{k_{sub}}{\sigma} \right) \Delta T_{max}} \right\} \quad (15)$$

The above expression can be equivalently referred to input to compute $V_{app,max}$:

$$V_{app,max} = \min \left\{ 2E_{BR,ox} \pi \epsilon_0 \epsilon_{ox} S_{el} \left(\frac{f}{\sigma} \right) \sqrt{1 + \alpha^2}, V_{ac,max}, I_{ac,max} \left(\frac{S_{el}}{n\sigma A_{el}} \right) \sqrt{1 + \left(\frac{1}{\alpha} \right)^2}, \sqrt{\beta \left(\frac{k_{sub}}{\sigma} \right) \Delta T_{max} \left[1 + \left(\frac{1}{\alpha} \right)^2 \right]} \right\} \quad (16)$$

As can be seen from all four constraints in equation 15, to maximize V_R , if not restricted by application requirements, it is best to use buffer solution with lowest available conductivity value. Setting the conductivity value would be a reasonable starting point in the design process, followed by deposition of nanometer-scale thin films and operating at highest frequency of excitation deliverable by the instruments. If limited by current delivery capability of instruments, one can consider reducing the number of the electrode fingers in the IDE configuration. Otherwise, in case a slight actuation delay can be tolerated, one can pattern multiple identical IDEs (arranged side-by-side) with proportionally less electrodes and simply switch through the IDEs and activate them consecutively. Furthermore, to reduce the temperature increase and to avoid bubble formation inside the channel, electrodes can be patterned on high thermal conductivity substrates (e.g. using silicon substrate with $k_{sub} = 149 \text{ Wm}^{-1}\text{K}^{-1}$ vs. Pyrex with $k_{sub} = 1.1 \text{ Wm}^{-1}\text{K}^{-1}$).

To complete our design methodology we should incorporate the above results in the context of our ultimate goal, i.e. maximizing the DEP force. We should note that tuning frequency of operation and conductivity of the buffer to achieve $V_{R,max}$ does not necessarily allow us to achieve maximum DEP force, $F_{DEP,max}$. To illustrate our point, it helps to recall the first order expression for DEP force that is acting on a dielectric sphere:

$$F_{DEP} = 2\pi \epsilon_0 \epsilon_m r^3 \text{Re}\{f_{CM}\} \nabla |E_{RMS}|^2 \quad (17)$$

where ε_m is the relative permittivity of the surrounding medium, r is the particle radius. The term f_{CM} in the above equation is the Clausius-Mossotti factor which is related to the effective polarizability of the particle with respect to that of the medium, and can be written as:

$$f_{CM} = \frac{\varepsilon_p^* - \varepsilon_m^*}{\varepsilon_p^* + 2\varepsilon_m^*} \quad (18)$$

where ε_p^* and ε_m^* are the relative complex permittivities of the particle and the medium respectively and both are frequency and conductivity dependent. The sign of the real part of the Clausius-Mossotti factor determines whether the particle is attracted to (positive DEP) or repelled from (nDEP) a region of high electric field strength. As can be seen from equations 17 and 18, F_{DEP} depends on both excitation frequency and conductivity of the buffer through f_{CM} and is proportional to the square of the electric field gradient, and equivalently, square of voltage V_R that is applied directly across the buffer. Therefore, in this context to achieve $F_{DEP,max}$ we should ensure that the conductivity of buffer and frequency of operation are selected such that $\text{Re}\{f_{CM}\}V_{R,max}^2$ is maximized. Figure 3(b) illustrates the corresponding $\text{Re}\{f_{CM}\}V_{R,max}^2$ values in the frequency vs. conductivity space which includes all the constraints and considerations that have been discussed so far.

Results and Discussions

Following our developed design guideline, we deposited 20 nm oxide layer, operated at relatively high frequency of 1 MHz, used a low-conductive solution as our wash buffer and excited the electrodes at 50 V_{pp} to ensure that we are not limited by thermal effects. To illustrate the application of this enhanced and robust DEP device, we demonstrated the multiplexed actuation capability of our device using an array of 16 IDE pairs patterned along a single channel. First, in order to validate the developed circuit model and test the functionality and electrical connectivity of each of the IDE pairs, we measured the impedance spectrum of IDEs and compared them with the spectrum predicted by the model. Figure 4(a) illustrates the overlaid impedance spectrum curves corresponding to the model and four

representative IDE pairs. The close agreement between the impedance spectrum curves for all IDEs ensures the same electrical capability and actuation performance across our array of electrodes.

To illustrate the robust multiplexed actuation capability of our device and 100% detachment of the protein-bound beads from each element of the array, we sequentially turned uDEP on by applying 50 V_{pp} (1 MHz) at the corresponding IDE pair. After each actuation step, we scanned other IDE pairs (with zero uDEP) to ensure their protein-bound beads have not been disturbed and remained attached to the surface (Figure 4(b)). We repeated the sequential actuation procedure, resulting in 100% bead detachment from each element of the array, with less than one-minute interval between each actuation step, to illustrate multiplex actuation capability in the time-span of a few minutes. This shows that for the envisioned immunoassay application, the amount of time required to sequentially actuate protein-bound beads, is shorter than the incubation time needed to perform such assays, and hence this approach does not significantly prolong the experiment.

In addition to multiplexed protein analysis, our platform enhances the DEP capability in statistical characterization of the force spectrum of biological interactions. The multiplexed format enables performing force spectroscopy on multiple IDEs independently, with high force dynamic range (given two orders of magnitude improvement in force strength offered by uDEP) in a single channel; minimizing inter-experiment variations that originate from disparities in buffer conditions and assay preparation steps. To illustrate this point, we repeated the IgG and anti-IgG assay procedure and ramped up the applied voltage at each of the IDE pairs one-by-one. For a given IDE and at each voltage (and hence F_{DEP}) increase step, we quantified the number of the detached beads to capture the detachment profile, as shown in Figure 5, which is informative of the distribution of binding forces that are holding the bead down to the surface through protein-protein interactions.

Given this force spectroscopy capability, our platform can be used to identify optimal buffer conditions or suitable reference force levels to differentiate between specific vs. non-specific interactions. For this application and using our device, we can study specific and non-specific interactions, by actuating specifically-bound beads (attached to the pre-functionalized IDEs) and non-

specifically-bound beads (attached to the ‘control’ non-functionalized IDEs) independently, all while operating in the same microfluidic channel, ensuring the same exact buffer conditions.

Having achieved a robust electrokinetic multiplexed actuating platform, future efforts will be focused on integrating an impedance sensor²⁶ downstream to quantify the detached beads electronically at each actuation step, and fully realize an integrated electronic system. Additionally, we will use this device to quantify and compare various protein-protein interactions, and also validate new protein biomarkers in biological samples. Overall, we envision a plethora of possibilities for performing rapid and inexpensive multiplexed protein analysis, using this electronic device, for applications ranging from biomarker validation and global protein analysis to diagnostics.

Methods

Fabrication

To create the microfluidic channel with 200 μm width, 50 μm height, and 3 cm length, the master mold was patterned onto a silicon substrate using SU-8 photoresist. Next, PDMS (10:1 prepolymer/curing agent) was poured onto the master mold and allowed to cure at 80 $^{\circ}\text{C}$ overnight. Once the PDMS channel was formed, it was peeled off from the mold. Then, to create the channel’s inlet and outlet ports, two holes (2 mm in diameter) were punched, one at each end.

To fabricate the electrodes, we used standard evaporation and lift-off processing techniques. Here, we patterned an array of 16 IDEs, where each element of the array was spaced 700 μm apart from one another. Each IDE was made up of 28 electrode pairs (i.e. $n = 28$). The Au/Cr electrodes (with width and spacing of 7 μm for both) were fabricated on a glass substrate. Then, to passivate our electrodes, we deposited a 20 nm SiO_2 film using Atomic Layer Deposition (ALD) Fiji F202 system from Cambridge Nanotech. For this purpose, with the wafers transferred to the reaction chamber, high purity Ar was used as a carrier gas. Consecutive pulses of Tris[dimethylamino]Silane and O_2 plasma were

generated, for a duration of 0.3 s and 20 s (at 300 W) respectively, achieving an effective deposition rate of 0.7 Å/cycle at 200 °C.

The PDMS microchannel and the oxide-deposited substrate containing the array of IDEs were then aligned and bonded together after standard oxygen plasma treatment, as the last step to create our device. This microfabricated device was then mounted onto a printed circuit board (PCB, Sierra Circuits Inc.) with an array of 16 switches dedicated to drive and control the electrical excitation of the corresponding IDEs patterned on the device. To interface the board with the device, we used a flex-PCB connector in conjunction with 3M z-axis adhesive film for flex-to-glass bonding. This interface solution worked well in our case. However, if we gear the platform for higher multiplexing (larger number of IDEs along the channel) and higher throughput (realized through parallel microfluidic channels, each containing an array of IDEs) applications, the density of electrode-electronics connections could become an issue. In that case, we have to resort to more sophisticated packaging solutions.

Sample Preparation and Surface Chemistry

To demonstrate the multiplexed functionality in eluting specifically-bound beads from the surface we chose anti-IgG and IgG interactions. As was shown previously, anti-IgG-IgG interaction is on the same order of magnitude in strength as typical antibody-antigen interactions^{15, 21}. To perform this assay, 2.8 μm-diameter goat anti-mouse IgG covered beads were used (initially in 0.5% w/v suspension). 500 μL of this solution was washed with PBS (containing 1% Bovine Serum Albumin, BSA and 0.05% Tween) and resuspended in 100 μL of 30x-diluted PBS. To physically adsorb IgG molecules on the channel surface, mouse IgG (originally 2 mg/mL, diluted by ×100) was incubated in the channel for 20 minutes. Then, to eliminate non-specific binding, we introduced BSA (1 mg/ml) in the channel. The channel was flushed and filled with diluted PBS, prior to loading the anti-IgG beads, and performing the experiment. To test for binding specificity, and as a control experiment, the above steps were performed on a separate chip, minus the physical adsorption of mouse IgG, to ensure that non-specific binding is minimized in our assay.

Experiment Setup

The flow rate in the channel was controlled using a syringe pump (Harvard Apparatus, USA). To measure the impedance spectrum and validate the IDEs, we used an impedance spectroscopy (Zurich Instruments HF2IS, Switzerland) and a transimpedance amplifier (Zurich Instruments HF2TA, Switzerland). This impedance spectroscopy was also used as a signal generator and input to a high voltage 50 V/V amplifier (Trek 2100HF, USA) to excite the electrodes with sine wave at 1 MHz.

Conclusions

In conclusion, we have presented a methodological approach to analyze an enhanced DEP system from both a circuit analysis and an electrothermal view points. In our developed model, we have taken into account various phenomena and constraints such as voltage degradation (due to the presence of oxide layer), oxide breakdown, instrumentation limitations, and temperature. While we performed our analysis and simulations based on the device geometry we fabricated, the principles used in this work can be extended to a wide variety of geometries and buffer conditions in the general context of high ac voltage microsystems.

The results from this analysis were used to develop a robust multiplexed bead-based protein assay platform, which can also be potentially used to perform force spectroscopy on protein-protein interactions. The use of high voltage tolerant corrosion-proof uDEP electrodes in modulating the protein-bound beads was necessary to enhance the DEP force such that to overcome protein-protein interactions that are on the order of a few hundred pico-Newtons.

To perform multiplexed bead-based assay, we patterned an array of 16 uDEP devices along a single microchannel. By selectively applying voltage at each uDEP electrodes, we sequentially detached protein-bound beads from the surface of IDEs. In addition to multiplexed protein analysis, we illustrated the capability of our multiplexed uDEP platform in statistical characterization of the force

spectrum of biological interactions. The enhanced DEP force strength allows higher dynamic range of actuation, as compared to the case with the non-uDEP (conventional DEP) IDEs of equivalent dimensions. Furthermore, the multiplexed format (each IDE dedicated to a specific interaction) along a single channel allows independent actuation of various interactions in a single microchannel, ensuring operation under the same buffer conditions; minimizing inter-experiment variations.

Future efforts will be focused on investigating the limits of using buffer properties (given its role in heat generation) to distinguish various interactions between proteins as well as gearing the multiplexed platform to study other antigen-antibody pair interactions. In parallel we will develop an electronic multiplexed protein biosensor, where we integrate the impedance sensor as a counter downstream to quantify the detached beads at each actuation step. This system will be ultimately used to detect a panel of protein biomarkers in human samples and will undoubtedly have a large impact on clinical medicine by equipping clinicians with a point-of-care diagnostic tool to provide personalized healthcare for their patients.

Acknowledgement

The authors would like to thank Dr. Kavusi for his guidance on the PCB implementation aspect of the system and Professor Santiago (Mechanical Engineering Department, Stanford University) for his valuable feedback on the developed electrothermal model of the device. Furthermore, the authors would like to thank Dr. Tayebi and Dr. Provine for sharing knowledge and expertise with regards to the fabrication process. This work was supported by the National Institutes of Health through grant PO1HG000205 and Natural Sciences and Engineering Research Council of Canada Scholarship through graduate tuition support. All authors contributed to manuscript preparation. S. Emaminejad and M. Javanmard set up the simulation platform, fabricated the microfluidic devices, and performed the experiments.

References

1. DeForge, L.; Remick, D., Sandwich ELISA for detection of picogram quantities of interleukin-8. *Immunological investigations* **1991**, *20* (1), 89-97.
2. MacBeath, G., Protein microarrays and proteomics. *nature genetics* **2002**, *32*, 526-532.
3. Esfandyarpour, R.; Esfandyarpour, H.; Harris, J. S.; Davis, R. W., Simulation and fabrication of a new novel 3D injectable biosensor for high throughput genomics and proteomics in a lab-on-a-chip device. *Nanotechnology* **2013**, *24* (46), 465301.
4. Esfandyarpour, R.; Esfandyarpour, H.; Javanmard, M.; Harris, J. S.; Davis, R. W., Microneedle biosensor: A method for direct label-free real time protein detection. *Sensors and Actuators B: Chemical* **2012**.
5. Esfandyarpour, R.; Javanmard, M.; Koochak, Z.; Esfandyarpour, H.; Harris, J. S.; Davis, R. W., Label-free electronic probing of nucleic acids and proteins at the nanoscale using the nanoneedle biosensor. *Biomicrofluidics* **2013**, *7* (4), 044114.
6. Esfandyarpour, R.; Esfandyarpour, H.; Javanmard, M.; Harris, J. S.; Davis, R. W. In *Electrical Detection of Protein Biomarkers Using Nanoneedle Biosensors*, MRS Proceedings, Cambridge Univ Press: 2012; pp mrsf11-1414-hh04-04.
7. Javanmard, M.; Davis, R., A microfluidic platform for electrical detection of DNA hybridization. *Sensors and Actuators B: Chemical* **2011**, *154* (1), 22-27.
8. Javanmard, M.; Esfandyarpour, H.; Pease, F.; Davis, R., Electrical detection of proteins and DNA using bioactivated microfluidic channels: Theoretical and experimental considerations. *Journal of Vacuum Science & Technology B: Microelectronics and Nanometer Structures* **2009**, *27* (6), 3099-3103.
9. Javanmard, M.; Talasaz, A. H.; Nemat-Gorgani, M.; Huber, D. E.; Pease, F.; Ronaghi, M.; Davis, R. W., A microfluidic platform for characterization of protein-protein interactions. *Sensors Journal, IEEE* **2009**, *9* (8), 883-891.
10. Javanmard, M.; Talasaz, A. H.; Nemat-Gorgani, M.; Pease, F.; Ronaghi, M.; Davis, R. W., Electrical detection of protein biomarkers using bioactivated microfluidic channels. *Lab on a Chip* **2009**, *9* (10), 1429-1434.
11. Mulvaney, S.; Myers, K.; Sheehan, P.; Whitman, L., Attomolar protein detection in complex sample matrices with semi-homogeneous fluidic force discrimination assays. *Biosensors and Bioelectronics* **2009**, *24* (5), 1109-1115.
12. Gaster, R. S.; Hall, D. A.; Nielsen, C. H.; Osterfeld, S. J.; Yu, H.; Mach, K. E.; Wilson, R. J.; Murmann, B.; Liao, J. C.; Gambhir, S. S., Matrix-insensitive protein assays push the limits of biosensors in medicine. *Nature medicine* **2009**, *15* (11), 1327-1332.
13. Kim, J.; Jensen, E. C.; Megens, M.; Boser, B.; Mathies, R. A., Integrated microfluidic bioprocessor for solid phase capture immunoassays. *Lab on a Chip* **2011**, *11* (18), 3106-3112.
14. Wang, H.; Chen, Y.; Hassibi, A.; Scherer, A.; Hajimiri, A. In *A frequency-shift CMOS magnetic biosensor array with single-bead sensitivity and no external magnet*, Solid-State Circuits Conference-Digest of Technical Papers, 2009. ISSCC 2009. IEEE International, IEEE: 2009; pp 438-439,439 a.
15. Javanmard, M.; Babrzadeh, F.; Davis, R., Microfluidic force spectroscopy for characterization of biomolecular interactions with piconewton resolution. *Applied physics letters* **2010**, *97* (17), 173704-173704-3.
16. Block, S. M.; Goldstein, L. S.; Schnapp, B. J., Bead movement by single kinesin molecules studied with optical tweezers. **1990**.
17. Ribeck, N.; Saleh, O. A., Multiplexed single-molecule measurements with magnetic tweezers. *Review of Scientific Instruments* **2008**, *79* (9), 094301-094301-6.
18. Emaminejad, S.; Javanmard, M.; Dutton, R. W.; Davis, R. W. In *Smart Surfaces: Use of Electrokinetics for Selective Modulation of Biomolecular Affinities*, MRS Proceedings, Cambridge Univ Press: 2012; pp mrsf11-1415-ii08-07.

19. Emaminejad, S.; Javanmard, M.; Dutton, R. W.; Davis, R. W., Smart Surface for Elution of Protein–Protein Bound Particles: Nanonewton Dielectrophoretic Forces Using Atomic Layer Deposited Oxides. *Analytical chemistry* **2012**, *84* (24), 10793-10801.
20. Emaminejad, S.; Javanmard, M.; Dutton, R. W.; Davis, R. W., Ultra Dielectrophoresis Using Atomic Layer Deposited Films: Electrothermal Analysis. *ECS Transactions* **2013**, *58* (10), 67-72.
21. Javanmard, M.; Emaminejad, S.; Dutton, R. W.; Davis, R. W., Use of negative dielectrophoresis for selective elution of protein-bound particles. *Analytical chemistry* **2012**, *84* (3), 1432-1438.
22. Javanmard, M.; Emaminejad, S.; Gupta, C.; Provine, J.; Davis, R.; Howe, R., Depletion of Cells and Abundant Proteins from Biological Samples by Enhanced Dielectrophoresis. *Sensors and Actuators B: Chemical* **2013**.
23. Emaminejad, S.; Javanmard, M.; Dutton, R. W.; Davis, R. W., Microfluidic diagnostic tool for the developing world: Contactless impedance flow cytometry. *Lab on a Chip* **2012**, *12* (21), 4499-4507.
24. Ramos, A.; Morgan, H.; Green, N.; Castellanos, A., Ac electrokinetics: a review of forces in microelectrode structures. *Journal of Physics D: Applied Physics* **1998**, *31* (18), 2338.
25. Wang, D.; Sigurdson, M.; Meinhart, C. D., Experimental analysis of particle and fluid motion in ac electrokinetics. *Experiments in fluids* **2005**, *38* (1), 1-10.
26. Mok, J.; Mindrinos, M.; Davis, R. W.; Javanmard, M., A Digital Microfluidic Protein Assay. *Proceedings of the National Academy of Sciences USA* **In Press**.

Figures

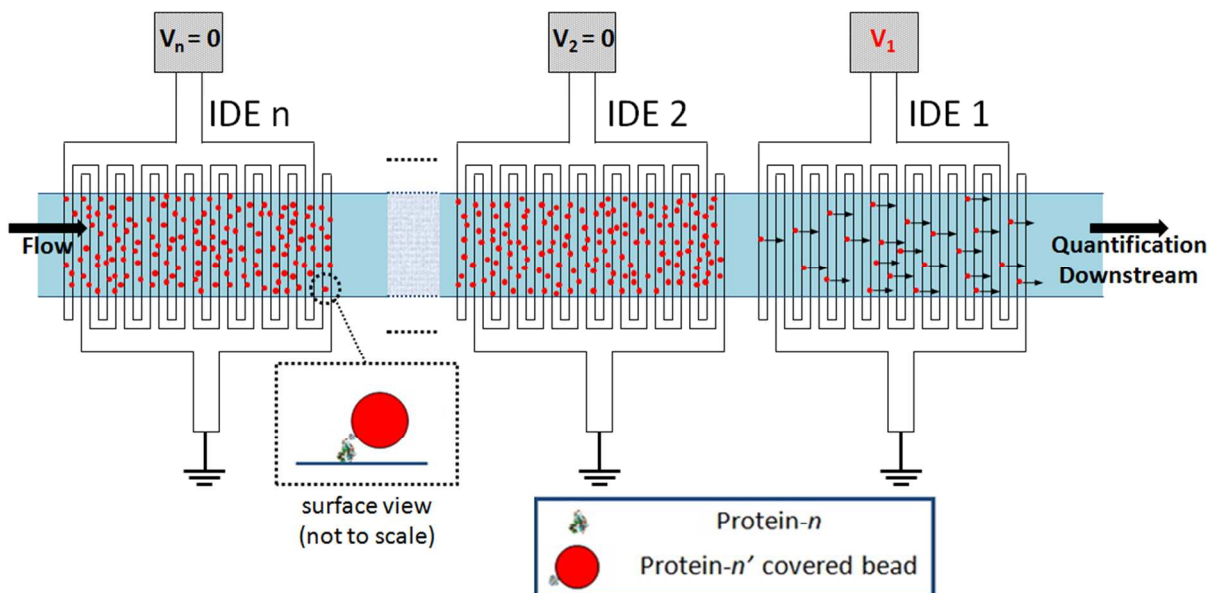
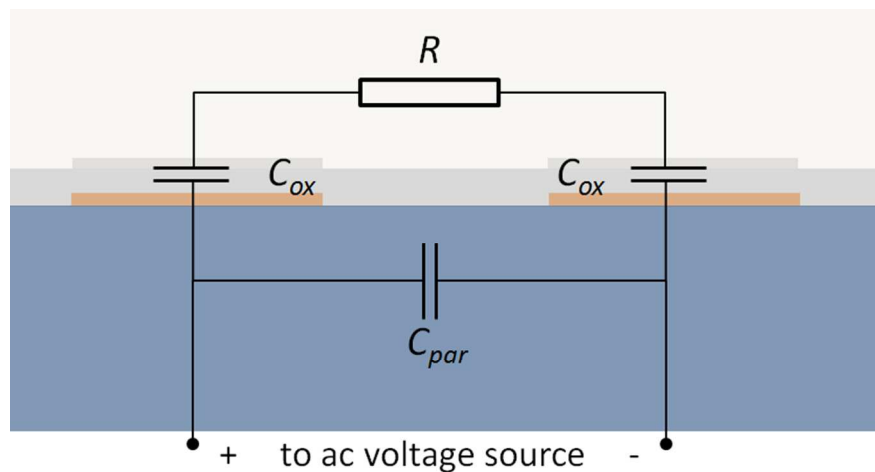
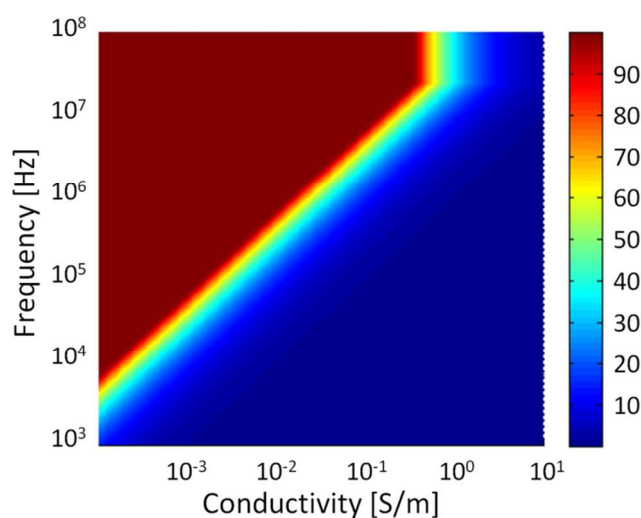


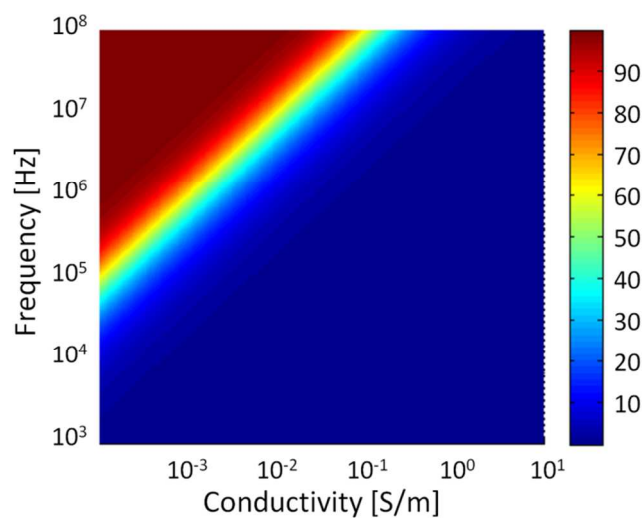
Figure 1: Bead-based multiplexed assay. Each element of array in the capture region is functionalized with a different protein, each targeting a specific protein that is coated on the micron-sized beads. Specifically bound beads on each element of the array are eluted selectively from the array and are quantified downstream (one element at a time). Here, applying voltage V_1 produces uDEP force, which in turn detaches the specifically bound beads from the surface of the 1st interdigitated electrode pair (i.e. IDE 1). With no voltage applied at the other IDEs, the protein-bound beads on the respective elements remain attached to the surface.



(a)

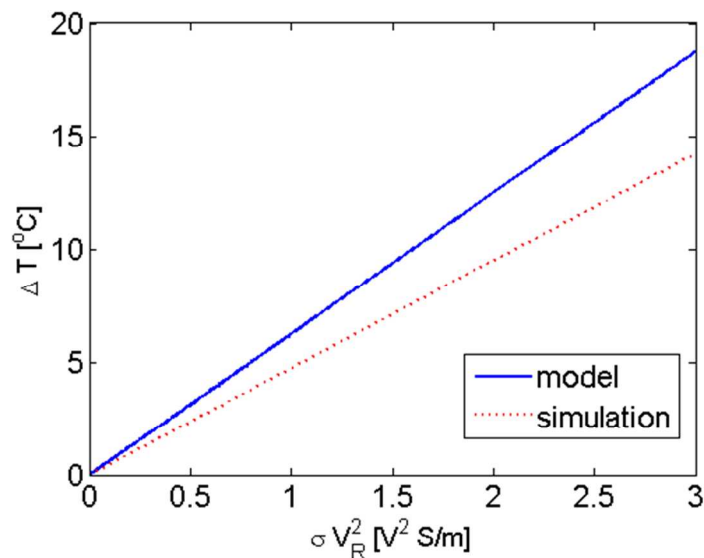


(b)

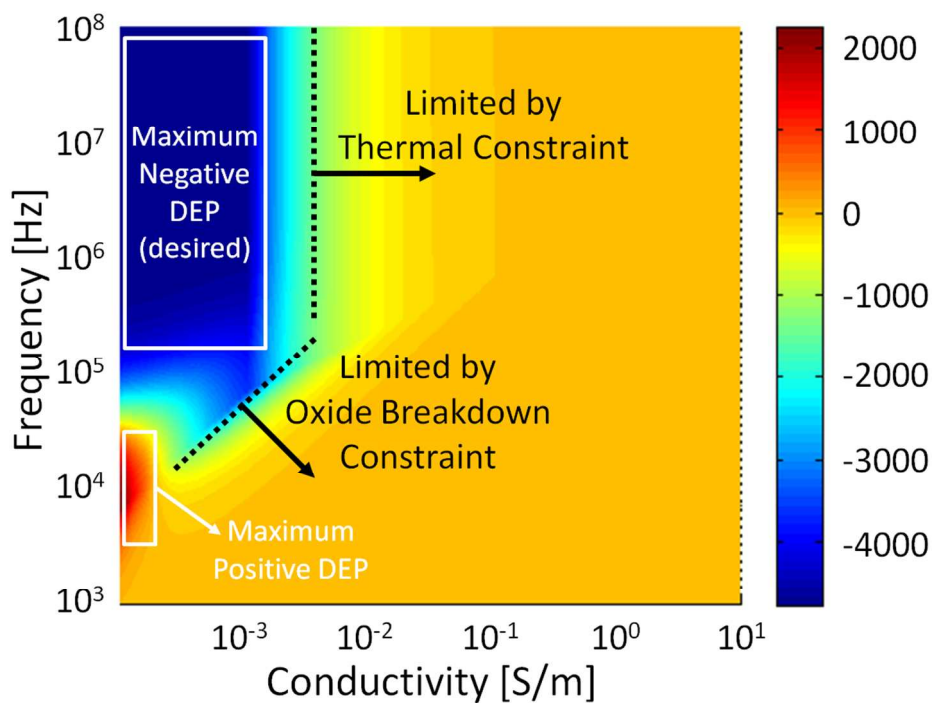


(c)

Figure 2: (a) Simplified electrical circuit model of two neighboring electrodes in an IDE pair. Conductive solution is modeled as resistance (R). The capacitance of the deposited oxide layer for each electrode-oxide-electrolyte interface is denoted by C_{ox} . The electrode coupling is modeled as parasitic capacitance C_{par} (b,c) Representative design space illustrating $V_{R,max}$ for (b) $t_{ox} = 10$ nm and (c) 1000 nm, while meeting the oxide breakdown criterion ($E_{BR,ox} = 1$ V/nm) and instrumentation limitation ($V_{ac,max} = 100$ V, $I_{ac,max} = 0.2$ A), in the f vs. σ space (assumed $7 \mu\text{m}$ wide and $7 \mu\text{m}$ spaced electrodes).



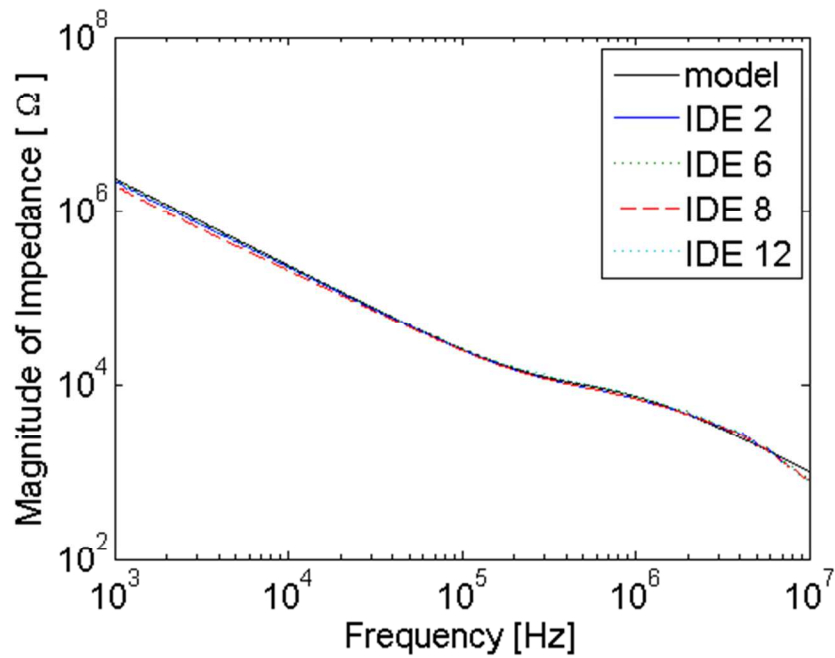
(a)



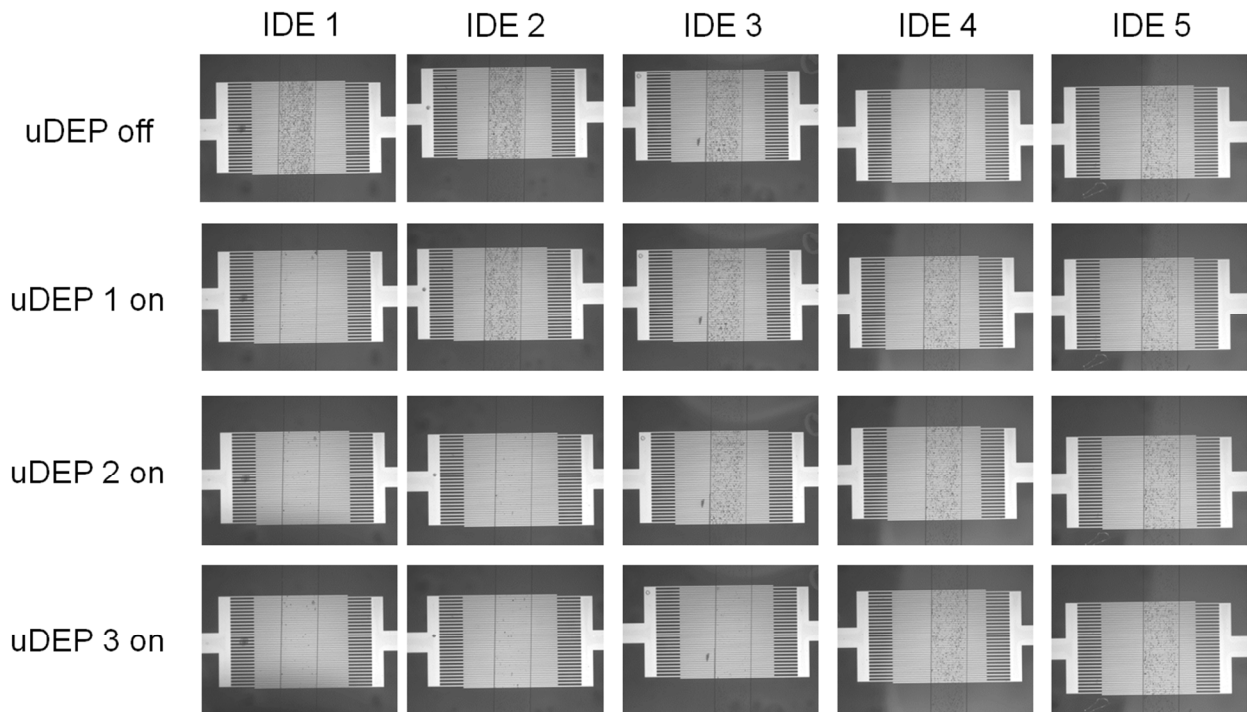
(b)

Figure 3: (a) Proportionality of the raise in temperature with the generated power density (setting an upper-bound on σV_R^2). By adjusting the value of β through calibration with simulation (in our case increased by $\sim 30\%$) we can precisely model the thermal behavior of the coplanar configuration. Here, we assumed $k_{sub} = 1.1 \text{ Wm}^{-1}\text{K}^{-1}$ and $t_{sub} = 100 \text{ }\mu\text{m}$. (b) Representative design space illustrating relative maximum DEP force (proportional to $\text{Re}\{f_{CM}\}V_{R,max}^2$) for a 10-nm deposited oxide that can be achieved for $7 \text{ }\mu\text{m}$ wide and $7 \text{ }\mu\text{m}$ spaced IDE pair geometry while meeting the design constraints. The

limitations imposed by the dominant design constraints are annotated on the graph. -/+ values correspond to negative/positive DEP. For our application we prefer the most negative value.



(a)



(b)

Figure 4: (a) Modeled vs. measured impedance spectrum of four representative IDEs. (b) Micrographs of five neighboring IDEs 1-5, where initially uDEP was off for all IDEs (row 1), and then uDEP was sequentially turned on by applying voltage at IDEs 1,2, and 3 (corresponding to rows 2,3, and 4).

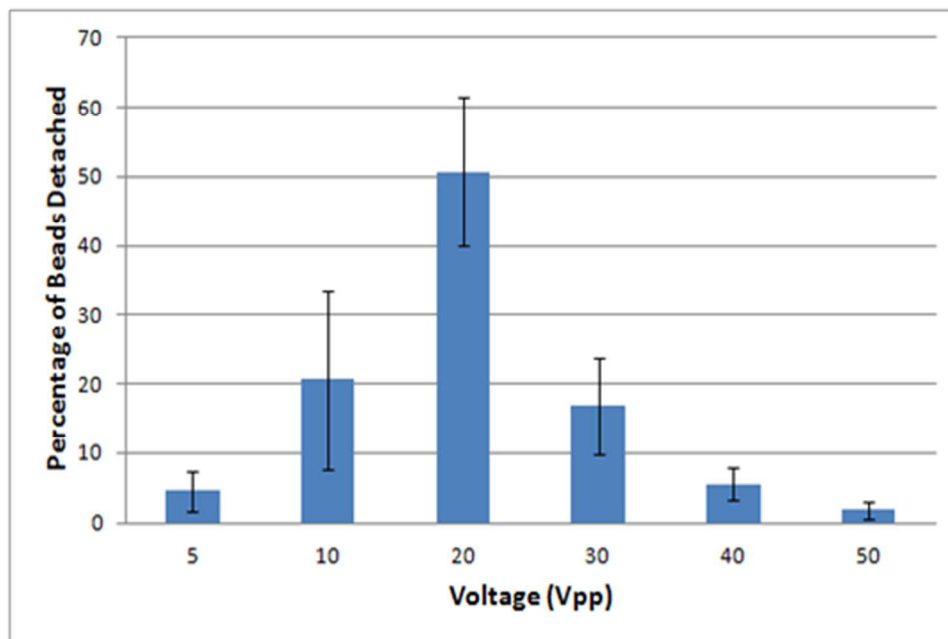


Figure 5: Detachment percentage of protein-bound beads when ramping up the applied voltage at each of the IDE pairs one-by-one. The results represent the collective detachment profile when actuating anti-IgG-IgG bound beads using our 16-plex platform. The array format allows performing force spectroscopy multiple times while ensuring operation under the same buffer conditions and assay preparation steps (DEP force is proportional to the square of the applied voltage).

For TOC Only:

With the aid of ultra-dielectrophoresis we demonstrated a robust electronic actuation system to perform a multiplexed bead-based protein assay.

